Progress In Electromagnetics Research, Vol. 143, 385–404, 2013

A NEW 2D NON-SPURIOUS DISCONTINUOUS GALERKIN FINITE ELEMENT TIME DOMAIN (DG-FETD) METHOD FOR MAXWELL'S EQUATIONS

Qiang Ren[1], Luis E. Tobón[1, 2], and Qing Huo Liu[1, *]

[1]Department of Electrical and Computer Engineering, Duke University, Durham, NC 27708, USA

[2]Department of Computer Science and Engineering, Pontificia Universidad Javeriana-Cali, Santiago de Cali 56710, Colombia

Abstract—A new discontinuous Galerkin Finite Element Time Domain (DG-FETD) method for Maxwell's equations is developed. It can suppress spurious modes using basis functions based on polynomials with the same order of interpolation for electric field intensity **E** and magnetic flux density **B**. Compared to FETD based on **EH** scheme, which requires different orders of interpolation polynomials for electric and magnetic field intensities, this method uses fewer unknowns and reduces the computation load. The discontinuous Galerkin method is employed to implement domain decomposition for the **EB** scheme based FETD. In addition, a well-posed time-domain perfectly matched layer (PML) is extended to the **EB** scheme to simulate the unbounded problem. Leap frog method is utilized for explicit time stepping. Numerical results demonstrate that the above proposed methods are effective and efficient for 2D time domain TMz multi-domain problems.

1. INTRODUCTION

The finite element method (FEM) has received significant attention in computational electromagnetics during the last three decades and has become one of the most widely used numerical methods for electromagnetics problems both in engineering and scientific research [1–7]. Recently, much progress has been made in Finite Element Time Domain (FETD) method [8–12], which extends the

Received 9 October 2013, Accepted 3 November 2013, Scheduled 18 November 2013

* Corresponding author: Qing Huo Liu (qhliu@ee.duke.edu).

FEM to time domain. It inherits the advantages of meshing flexibility, material generality and matrices sparseness from FEM and advantages of performing wideband analysis, simulating non-linear and transient phenomena from the time domain method.

FETD can be implemented in two ways, one based on the curl-curl second order wave equation [13–16] and the other based on the first order Maxwell's equations [17–20]. The former one can use the relatively plenty of research results from frequency domain FEM, such as the choice of basis functions and stability analysis, however, it is difficult to implement the perfectly matched layer (PML) as an absorbing boundary condition. The latter one based on first order Maxwell's curl equations is more suitable to use a well-posed PML when an unbounded region is simulated. The FETD based on electric field intensity **E** and magnetic flux density **B** has been developed in [21, 22]. This method works very well and has been combined with nonlinear circuit solvers [23, 24].

On the other hand, the FETD method can be also developed using **E** and **H** as field variables. Then, both **E** and **H** fields must use edge based basis functions in order to satisfy the continuity conditions for the tangential field components across element interfaces. However, this **EH** scheme has the problem of spurious modes, i.e., modes which are non-physical. These non-physical solutions appear when the same order of basis functions are used for **E** and **H**, for example, $\mathbf{E}_n\mathbf{H}_n$ (n-th order basis functions for both **E** and **H**) [25, 26]. Because **H** and **E** have the same continuous condition on the tangential components, **H** will not be compatible with the nullspace of the curl operator if **H** and **E** also have the same order. To suppress the spurious modes, different orders of interpolation polynomials should be employed, for example, $\mathbf{E}_n\mathbf{H}_{n+1}$ (n-th and $(n+1)$-th order basis functions for **E** and **H** respectively) or $\mathbf{E}_{n+1}\mathbf{H}_n$ ($(n+1)$-th and n-th order basis functions for **E** and **H** respectively) [27–29]. Numerical results have shown that this FETD method based on the **E** and **H** fields works well, although at the expense of more unknowns than the $\mathbf{E}_n\mathbf{H}_n$ scheme.

One drawback of the FETD method, compared to the FDTD method, is its need to invert a large sparse matrix. To overcome this, Domain Decomposition Method (DDM) can be used in FETD to further enhance the computation efficiency. In previous FETD research, discontinuous Galerkin method has been employed to implement DDM based on the **EH** scheme for large-scale problems where the inversion of a large mass matrix is too expensive. This method has been shown useful as the tangential continuous basis functions for **E** and **H** naturally satisfy the requirements by the numerical flux [28, 30–35]. However, the **EH** scheme needs more

unknowns than the **EB** scheme. Therefore, a combination of **EB** scheme based FETD and discontinuous Galerkin method is proposed for the first time to further accelerate simulation. This is the first new contribution of this work. The second new contribution of this work is the application of a strongly well posed perfectly matched layer (PML) in the FETD with **E** and **B** fields.

2. PROBLEM STATEMENT AND RESEARCH GOAL

The governing equations are the first order Maxwell's curl equations with electric field intensity **E** and magnetic flux density **B** as the variables

$$\epsilon \frac{\partial \mathbf{E}}{\partial t} = \nabla \times \mu^{-1}\mathbf{B} - \sigma_e \mathbf{E} - \mathbf{J} \tag{1}$$

$$\frac{\partial \mathbf{B}}{\partial t} = -\nabla \times \mathbf{E} - \sigma_m \mu^{-1}\mathbf{B} - \mathbf{M} \tag{2}$$

where ϵ, μ, σ_e, and σ_m denote material's permittivity, permeability, electric conductivity and magnetic conductivity, respectively. **J** and **M** are electric current density and magnetic current density due to the imposed sources.

The goal in this research can be divided into 3 parts:

- Analyze the eigenvalues of FETD to show the effectiveness of **EB** scheme to suppress the spurious modes with the same order basis functions for **E** and **B**. Advantages of the **EB** scheme in computation costs can be shown via comparison to the **EH** scheme.
- Apply the strongly well-posed PML to **EB** scheme FETD and find the optimal thickness of PML, which will provide a guidance for future possible applications with unbounded problems.
- As the **EB** scheme is advantageous, the DG-FETD based on **EB** scheme can be implemented to further enhance the computation efficiency compared to single domain **EB** scheme FETD.

Details of these three parts are elaborated in the following sections.

3. FORMULATION

To solve (1) and (2), curl-conforming vector basis functions are used to discretize **E**, and divergence-conforming vector basis functions are used to discretize **B**. These basis functions are from the first and second families of Nedlec elements, i.e., the edge elements and face elements [36, 37], respectively.

In FETD, reference elements are introduced to make the code more generalizable and easier to debug. We denote the curl-conforming basis functions for $\mathbf{E}$ as $\mathbf{\Phi}$ and $\hat{\mathbf{\Phi}}$ in the physical and reference domains, respectively, and denote the divergence-conforming basis functions for $\mathbf{B}$ as $\mathbf{\Psi}$ and $\hat{\mathbf{\Psi}}$ in the physical and reference domains, respectively.

To transform the basis functions from reference domain to physical domain, covariant and contravariant projections are needed [38], which can be expressed as

$$\mathbf{\Phi} = \mathbf{J}_a^{-1}\hat{\mathbf{\Phi}} \qquad \nabla \times \mathbf{\Phi} = \frac{1}{|\mathbf{J}_a|}\mathbf{J}_a^T\hat{\nabla} \times \hat{\mathbf{\Phi}} \tag{3}$$

$$\mathbf{\Psi} = \frac{1}{|\mathbf{J}_a|}\mathbf{J}_a^T\hat{\mathbf{\Psi}} \qquad \nabla \times \mathbf{\Psi} = \mathbf{J}_a^{-1}\hat{\nabla} \times \hat{\mathbf{\Psi}} \tag{4}$$

where

$$\hat{\nabla} = \frac{\partial}{\partial\xi}\hat{\xi} + \frac{\partial}{\partial\eta}\hat{\eta} + \frac{\partial}{\partial\zeta}\hat{\zeta} \tag{5}$$

and $\mathbf{J}_a$ is the Jacobian matrix defined as

$$\mathbf{J}_a = \begin{bmatrix} \frac{\partial x}{\partial\xi} & \frac{\partial y}{\partial\xi} & \frac{\partial z}{\partial\xi} \\ \frac{\partial x}{\partial\eta} & \frac{\partial y}{\partial\eta} & \frac{\partial z}{\partial\eta} \\ \frac{\partial x}{\partial\zeta} & \frac{\partial y}{\partial\zeta} & \frac{\partial z}{\partial\zeta} \end{bmatrix} \tag{6}$$

x, y, z are the coordinates in the physical domain, and ξ, η, ζ are the coordinates in the reference domain.

3.1. The EB Scheme Based FETD Method

3.1.1. Single Domain with PML Region

The compact vector form Maxwell's equations for the strongly well-posed PML region are given by Fan and Liu [39]

$$\nabla\times\tilde{\mathbf{E}} = -\frac{\partial\tilde{\mathbf{B}}}{\partial t} - (\sigma_m\mu^{-1}+\mathbf{\Lambda}_1)\tilde{\mathbf{B}} - (\sigma_m\mu^{-1}\mathbf{\Lambda_1}+\mathbf{\Lambda}_2)\mathbf{B}^{(1)} - \sigma_m\mu^{-1}\mathbf{\Lambda}_3\mathbf{B}^{(2)} \tag{7}$$

and

$$\nabla\times\mu^{-1}\tilde{\mathbf{B}} = \epsilon\frac{\partial\tilde{\mathbf{E}}}{\partial t} + (\sigma_e+\epsilon\mathbf{\Lambda}_1)\tilde{\mathbf{E}} + (\sigma_e\mathbf{\Lambda}_1+\epsilon\mathbf{\Lambda}_2)\mathbf{E}^{(1)} + \sigma_e\mathbf{\Lambda}_3\mathbf{E}^{(2)} \tag{8}$$

The auxiliary time-integrated fields are governed by ordinary partial differential equations

$$\frac{\partial \mathbf{E}^{(1)}}{\partial t} = \tilde{\mathbf{E}} - \mathbf{\Lambda}_0 \mathbf{E}^{(1)} \qquad \frac{\partial \mathbf{E}^{(2)}}{\partial t} = \mathbf{E}^{(1)} \tag{9}$$

$$\frac{\partial \mathbf{B}^{(1)}}{\partial t} = \tilde{\mathbf{B}} - \mathbf{\Lambda}_0 \mathbf{B}^{(1)} \qquad \frac{\partial \mathbf{B}^{(2)}}{\partial t} = \mathbf{B}^{(1)} \tag{10}$$

where

$$\tilde{\mathbf{B}} = \mathbf{B} + \mathbf{\Lambda}_0 \mathbf{B}^{(1)} \qquad \tilde{\mathbf{E}} = \mathbf{E} + \mathbf{\Lambda}_0 \mathbf{E}^{(1)} \tag{11}$$

$$\mathbf{\Lambda}_0 = \mathrm{diag}\{\omega_x, \omega_y, \omega_z\} \tag{12}$$

$$\mathbf{\Lambda}_1 = \mathrm{diag}\{(\omega_y + \omega_z - \omega_x)(\omega_x + \omega_z - \omega_y), (\omega_y + \omega_z - \omega_x)\} \tag{13}$$

$$\mathbf{\Lambda}_2 = \mathrm{diag}\{(\omega_x - \omega_y)(\omega_x - \omega_z), (\omega_y - \omega_x)(\omega_y - \omega_z), (\omega_z - \omega_x)(\omega_z - \omega_y)\} \tag{14}$$

$$\mathbf{\Lambda}_3 = \mathrm{diag}\{\omega_y\omega_z, \omega_x\omega_z, \omega_x\omega_y\} \tag{15}$$

ω_η is the attenuation coefficient in the direction η ($\eta = x, y, z$). $\tilde{\mathbf{B}}$, $\mathbf{B}^{(1)}$, $\mathbf{B}^{(2)}$ are expanded with the same divergence-conforming basis functions, and $\tilde{\mathbf{E}}$, $\mathbf{E}^{(1)}$, $\mathbf{E}^{(2)}$ are expanded with the same curl-conforming basis functions, that is, $\tilde{\mathbf{B}} = \sum \tilde{b}_i \mathbf{\Psi}_\mathbf{i}$, $\mathbf{B}^{(1)} = \sum b_i^{(1)} \mathbf{\Psi}_i$, $\mathbf{B}^{(2)} = \sum b_i^{(2)} \mathbf{\Psi}_i$, $\tilde{\mathbf{E}} = \sum \tilde{e}_i \mathbf{\Phi}_i$, $\mathbf{E}^{(1)} = \sum e_i^{(1)} \mathbf{\Phi}_i$, $\mathbf{E}^{(2)} = \sum e_i^{(2)} \mathbf{\Phi}_i$.

Applying the Galerkin's method to (7), (8) and combining them to (9)–(11), the discretized system with PML is as below:

$$\begin{bmatrix} \mathbf{M}_{\tilde{e}\tilde{e}} & & & & & & \\ & \mathbf{M}_{\tilde{b}\tilde{b}} & & & & & \\ & & \mathbf{I} & & & & \\ & & & \mathbf{M}_{b^{(1)}b^{(1)}} & & & \\ & & & & \mathbf{I} & & \\ & & & & & \mathbf{I} & \end{bmatrix} \begin{bmatrix} \partial_t \tilde{\mathbf{e}} \\ \partial_t \tilde{\mathbf{b}} \\ \partial_t \mathbf{e}^{(1)} \\ \partial_t \mathbf{b}^{(1)} \\ \partial_t \mathbf{e}^{(2)} \\ \partial_t \mathbf{b}^{(2)} \end{bmatrix} = \begin{bmatrix} \mathbf{j} \\ \mathbf{m} \\ \\ \\ \\ \end{bmatrix}$$

$$+ \begin{bmatrix} \mathbf{C}_{\tilde{e}\tilde{e}} & \mathbf{K}_{\tilde{e}\tilde{b}} & \mathbf{C}_{\tilde{e}e^{(1)}} & & \mathbf{C}_{\tilde{e}e^{(2)}} & \\ \mathbf{K}_{\tilde{b}\tilde{e}} & \mathbf{C}_{\tilde{b}\tilde{b}} & & \mathbf{C}_{\tilde{b}b^{(1)}} & & \mathbf{C}_{\tilde{b}b^{(2)}} \\ \mathbf{I} & & \mathbf{C}_{e^{(1)}e^{(1)}} & & & \\ & \mathbf{C}_{b^{(1)}\tilde{b}} & & \mathbf{C}_{b^{(1)}b^{(1)}} & & \\ & & \mathbf{I} & & & \\ & & & \mathbf{I} & & \end{bmatrix} \begin{bmatrix} \tilde{\mathbf{e}} \\ \tilde{\mathbf{b}} \\ \mathbf{e}^{(1)} \\ \mathbf{b}^{(1)} \\ \mathbf{e}^{(2)} \\ \mathbf{b}^{(2)} \end{bmatrix} \tag{16}$$

where $\mathbf{I}$ is the identity matrix, and the blanks are filled with zeros.

Other elementary matrices in (16) are as follows

$$(\mathbf{M}_{\tilde{e}\tilde{e}})^e_{pq} = \langle \mathbf{\Phi}_p, \epsilon \mathbf{\Phi}_q \rangle_{V_e} \tag{17}$$

$$(\mathbf{M}_{b^{(1)}b^{(1)}})^e_{pq} = (\mathbf{M}_{\tilde{b}\tilde{b}})^e_{pq} = (\mathbf{C}_{b^{(1)}\tilde{b}})^e_{pq} = \langle \mathbf{\Psi}_p, \mathbf{\Psi}_q \rangle_{V_e} \tag{18}$$

$$(\mathbf{K}_{\tilde{e}\tilde{b}})^e_{pq} = \langle \mathbf{\Phi}_p, \nabla \times \mu^{-1} \mathbf{\Psi}_q \rangle_{V_e} \quad (\mathbf{K}_{\tilde{b}\tilde{e}})^e_{pq} = -\langle \mathbf{\Psi}_q, \nabla \times \mathbf{\Phi}_p \rangle_{V_e} \tag{19}$$

$$(C_{\tilde{e}e^{(1)}})^e_{pq} = -\langle \mathbf{\Phi}_p, (\sigma_e \mathbf{\Lambda}_1 + \epsilon \mathbf{\Lambda}_2) \mathbf{\Phi}_q \rangle_{V_e} \tag{20}$$

$$(\mathbf{C}_{\tilde{e}\tilde{e}})^e_{pq} = -\langle \mathbf{\Phi}_p, (\sigma_e + \epsilon \mathbf{\Lambda}_1) \mathbf{\Phi}_q \rangle_{V_e} \tag{21}$$

$$(\mathbf{C}_{\tilde{e}e^{(2)}})^e_{pq} = -\langle \mathbf{\Phi}_p, \sigma_e \mathbf{\Lambda}_3 \mathbf{\Phi}_q \rangle_{V_e} \quad (\mathbf{C}_{e^{(1)}e^{(1)}})^e_{pq} = -\langle \mathbf{\Phi}_p, \mathbf{\Lambda}_0 \mathbf{\Phi}_p \rangle_{V_e} \tag{22}$$

$$(\mathbf{C}_{\tilde{b}\tilde{b}})^e_{pq} = -\langle \mathbf{\Psi}_p, (\sigma_m \mu^{-1} + \mathbf{\Lambda}_1) \mathbf{\Psi}_q \rangle_{V_e} \tag{23}$$

$$(\mathbf{C}_{\tilde{b}b^{(1)}})^e_{pq} = -\langle \mathbf{\Psi}_p, (\sigma_m \mu^{-1} \mathbf{\Lambda}_1 + \mathbf{\Lambda}_2) \mathbf{\Psi}_q \rangle_{V_e} \tag{24}$$

$$(\mathbf{C}_{b^{(1)}b^{(1)}})^e_{pq} = -\langle \mathbf{\Psi}_p, \mathbf{\Lambda}_0 \mathbf{\Psi}_q \rangle_{V_e} \tag{25}$$

$$(\mathbf{C}_{\tilde{b}b^{(2)}})^e_{pq} = -\langle \mathbf{\Psi}_p, \sigma_m \mu^{-1} \mathbf{\Lambda}_3 \mathbf{\Psi}_q \rangle_{V_e} \tag{26}$$

The non-open cases are just special configurations of the above situation, the only difference is that $\mathbf{\Lambda}_0$, $\mathbf{\Lambda}_1$, $\mathbf{\Lambda}_2$ and $\mathbf{\Lambda}_3$ are set to 0.

3.2. Formulation of the EB Scheme Based DG-FETD

Assume the computational domain is divided into N subdomains. Denote the ith subdomain as the local subdomain, and jth as an adjacent one. Performing integration by parts with the Galerkin's weak form of Maxwell's equations for the local subdomain, we can obtain

$$\begin{aligned} &\int_V \mathbf{\Phi}_p^{(i)} \cdot \left(\epsilon \frac{\partial \mathbf{E}^{(i)}}{\partial t} + \sigma_e \mathbf{E}^{(i)} + \mathbf{J}^{(i)} \right) dV \\ &= \int_V \nabla \times \mathbf{\Phi}_p^{(i)} \cdot \mu^{-1} \mathbf{B}^{(i)} dV + \int_S \mathbf{\Phi}_p^{(i)} \cdot \left(\hat{\mathbf{n}}^{(i)} \times \mu^{-1} \mathbf{B}^{tot} \right) dS \end{aligned} \tag{27}$$

$$\begin{aligned} &\int_V \mathbf{\Psi}_p^{(i)} \cdot \left(\frac{\partial \mathbf{B}^{(i)}}{\partial t} + \sigma_m \mu^{-1} \mathbf{B}^{(i)} + \mathbf{M}^{(i)} \right) dV \\ &= -\int_V \nabla \times \mathbf{\Psi}_p^{(i)} \cdot \mathbf{E}^{(i)} dV - \int_S \mathbf{\Psi}_p^{(i)} \cdot \left(\hat{\mathbf{n}}^{(i)} \times \mathbf{E}^{tot} \right) dS \end{aligned} \tag{28}$$

where $(\cdot)^{(i)}$ represents the vector for the ith subdomain, $\hat{\mathbf{n}}^{(i)}$ is its outward normal vector on the boundary, and $(\cdot)^{tot}$ represents the total field. For the volume integration term, $(\cdot)^{tot} = (\cdot)^{(i)}$ and for the surface integration term, $(\cdot)^{tot}$ is from the contribution of both the ith subdomain and the jth subdomain.

To deal with $\hat{\mathbf{n}}^{(i)} \times \mathbf{E}^{tot}$ and $\hat{\mathbf{n}}^{(i)} \times \mu^{-1}\mathbf{B}^{tot}$, central flux is implemented, that is,

$$\left(\hat{\mathbf{n}}^{(i)} \times \mathbf{E}^{tot}\right) = \frac{1}{2}\left(\hat{\mathbf{n}}^{(i)} \times \mathbf{E}^{(i)} + \hat{\mathbf{n}}^{(i)} \times \mathbf{E}^{(j)}\right) \tag{29}$$

$$\left(\hat{\mathbf{n}}^{(i)} \times \mu^{-1}\mathbf{B}^{tot}\right) = \frac{1}{2}\left(\hat{\mathbf{n}}^{(i)} \times \frac{\mathbf{B}^{i}}{\mu^{(i)}} + \hat{\mathbf{n}}^{(i)} \times \frac{\mathbf{B}^{(j)}}{\mu^{(j)}}\right) \tag{30}$$

The discretized system for the ith subdomain is

$$\mathbf{M}_{ee}^{(i)}\frac{d\mathbf{e}^{(i)}}{dt} = \mathbf{K}_{eb}^{(i)}\mathbf{b}^{(i)} + \mathbf{C}_{ee}^{(i)}\mathbf{e}^{(i)} + \mathbf{j}^{(i)} + \sum_{j=1}^{N}\mathbf{L}_{eb}^{(ij)}\mathbf{e}^{(j)} \tag{31}$$

$$\mathbf{M}_{bb}^{(i)}\frac{d\mathbf{b}^{(i)}}{dt} = \mathbf{K}_{be}^{(i)}\mathbf{e}^{(i)} + \mathbf{C}_{bb}^{(i)}\mathbf{b}^{(i)} + \mathbf{m}^{(i)} + \sum_{j=1}^{N}\mathbf{L}_{be}^{(ij)}\mathbf{b}^{(j)} \tag{32}$$

where the mass matrices $\mathbf{M}_{eepq}^{(i)}$, $\mathbf{M}_{bbpq}^{(i)}$, the damping matrices $\mathbf{C}_{eepq}^{(i)}$, $\mathbf{C}_{bbpq}^{(i)}$ and the stiffness matrices $\mathbf{K}_{ebpq}^{(i)}$, $\mathbf{K}_{bepq}^{(i)}$ are the same as equations (17)–(19) and other elemental matrices are

$$\begin{aligned}
\left(\mathbf{L}_{eb}^{(ij)}\right)_{pq} &= \left\langle \mathbf{\Phi}_{p}^{(i)}, \left(\hat{\mathbf{n}}^{(i)} \times \frac{\mathbf{\Psi}_{q}^{(j)}}{\mu^{(j)}}\right)\right\rangle_{S_{ij}} \\
\left(\mathbf{L}_{be}^{(ij)}\right)_{pq} &= \left\langle \mathbf{\Psi}_{p}^{(i)}, \left(\hat{\mathbf{n}}^{(i)} \times \mathbf{\Phi}_{q}^{(j)}\right)\right\rangle_{S_{ij}}
\end{aligned} \tag{33}$$

$$\begin{aligned}
\left(\mathbf{L}_{eb}^{(ii)}\right)_{pq} &= \frac{1}{2}\sum_{j=1}^{N}\left\langle \mathbf{\Phi}_{p}^{(i)}, \left(\hat{\mathbf{n}}^{(i)} \times \frac{\mathbf{\Psi}_{q}^{(i)}}{\mu^{(i)}}\right)\right\rangle_{S_{ij}} \\
\left(\mathbf{L}_{be}^{(ii)}\right)_{pq} &= \frac{1}{2}\sum_{j=1}^{N}\left\langle \mathbf{\Psi}_{p}^{(i)}, \left(\hat{\mathbf{n}}^{(i)} \times \mathbf{\Phi}_{q}^{(i)}\right)\right\rangle_{S_{ij}}
\end{aligned} \tag{34}$$

S_{ij} is the interface between the ith and jth subdomains.

3.3. Time Stepping Scheme

The explicit leap frog is chosen as the time stepping scheme for FETD, in which the $\mathbf{E}$ and $\mathbf{B}$ use half step staggered grids in the temporal dimension. Compared to other explicit time stepping schemes such as Runge Kutta, leap frog is relatively easier to implement and it is also suitable for hybrid methods such as FDTD.

3.3.1. Leap Frog for the **EB** *Scheme Based FETD with PML*

In the leap frog for the **EB** scheme based FETD with PML, $\tilde{\mathbf{b}}$ is half step staggered with $\mathbf{b}^{(1)}$ and $\mathbf{b}^{(2)}$, while $\tilde{\mathbf{e}}$ is half step staggered with $\mathbf{e}^{(1)}$ and $\mathbf{e}^{(2)}$. One feasible updating sequence for the unknown vectors is as below

$$\mathbf{b}_n^{(1)} = \left(\frac{\mathbf{M}_{b^{(1)}b^{(1)}}}{\Delta t} - \frac{\mathbf{C}_{b^{(1)}b^{(1)}}}{2}\right)^{-1} \left[\left(\frac{\mathbf{M}_{b^{(1)}b^{(1)}}}{\Delta t} + \frac{\mathbf{M}_{b^{(1)}b^{(1)}}}{2}\right)\mathbf{b}_{n-1}^{(1)} + \mathbf{M}_{b^{(1)}\tilde{b}}\tilde{\mathbf{b}}_{n-\frac{1}{2}}\right] \tag{35}$$

$$\mathbf{b}_n^{(2)} = \mathbf{b}_{n-1}^{(2)} + \frac{\Delta t}{2}\left[\mathbf{b}_n^{(1)} + \mathbf{b}_{n-1}^{(1)}\right] \tag{36}$$

$$\tilde{\mathbf{b}}_{n+\frac{1}{2}} = \left(\frac{\mathbf{M}_{\tilde{b}\tilde{b}}}{\Delta t} - \frac{\mathbf{C}_{\tilde{b}\tilde{b}}}{2}\right)^{-1}\left[\left(\frac{\mathbf{M}_{\tilde{b}\tilde{b}}}{\Delta t} + \frac{\mathbf{C}_{\tilde{b}\tilde{b}}}{2}\right)\tilde{\mathbf{b}}_{n-\frac{1}{2}} + \mathbf{K}_{\tilde{b}\tilde{e}}\tilde{\mathbf{e}}_n + \mathbf{C}_{\tilde{b}b^{(1)}}\mathbf{b}_n^{(1)}\right] \tag{37}$$

$$\mathbf{e}_{n+\frac{1}{2}}^{(1)} = \mathbf{e}_{n-\frac{1}{2}}^{(1)} + \Delta t\tilde{\mathbf{e}}_n \qquad \mathbf{e}_{n+\frac{1}{2}}^{(2)} = \mathbf{e}_{n-\frac{1}{2}}^{(2)} + \Delta t\mathbf{e}_{n-\frac{1}{2}}^{(1)} + \frac{(\Delta t)^2}{2}\tilde{\mathbf{e}}_n \tag{38}$$

$$\tilde{\mathbf{e}}_{n+1} = \left(\frac{\mathbf{M}_{\tilde{e}\tilde{e}}}{\Delta t} - \frac{\mathbf{C}_{\tilde{e}\tilde{e}}}{2}\right)^{-1}\left[\left(\frac{\mathbf{M}_{\tilde{e}\tilde{e}}}{\Delta t} + \frac{\mathbf{C}_{\tilde{e}\tilde{e}}}{2}\right)\tilde{\mathbf{e}}_n + \mathbf{K}_{\tilde{e}\tilde{b}}\tilde{\mathbf{b}}_{n+\frac{1}{2}} + \mathbf{C}_{\tilde{e}e^{(1)}}\mathbf{e}_{n+\frac{1}{2}}^{(1)} + \mathbf{C}_{\tilde{e}e^{(2)}}\mathbf{e}_{n+\frac{1}{2}}^{(2)} + \mathbf{j}_{n+\frac{1}{2}}\right] \tag{39}$$

3.3.2. Leap Frog for the **EB** *Scheme Based DG-FETD*

In leap frog for the **EB** scheme based DG-FETD, the unknown vectors are updated in the subdomain-major sequence, that is, **b** and **e** of a certain subdomain are updated, then the next subdomain. The pseudo-code is as follows:

$$\begin{cases} \text{for } n = 1\text{: } N_t \\ \quad \text{for } i = 1\text{: } N_d \\ \quad\quad \mathbf{b}_{n+\frac{1}{2}}^{(i)} = \mathbf{b}_{n-\frac{1}{2}}^{(i)} + \Delta t\left(\mathbf{M}_{bb}^{(i)}\right)^{-1}\left[\mathbf{K}_{be}^{(i)}\mathbf{e}_n^{(i)} + \mathbf{C}_{bb}^{(i)}\mathbf{b}_{n-\frac{1}{2}}^{(i)} + \mathbf{M}_n^{(i)} + \sum_{j=1}^{N_d}\mathbf{L}_{be}^{(ij)}\mathbf{e}_n^{(j)}\right] \\ \quad\quad \mathbf{e}_{n+1}^{(i)} = \mathbf{e}_n^{(i)} + \Delta t\left(\mathbf{M}_{ee}^{(i)}\right)^{-1}\left[\mathbf{K}_{eb}^{(i)}\mathbf{b}_{n+\frac{1}{2}}^{i} + \mathbf{C}_{ee}^{(i)}\mathbf{e}_n^{(i)} + \mathbf{J}_n^{(i)} + \sum_{j=1}^{N_d}\mathbf{L}_{eb}^{(ij)}\mathbf{b}_n^{(j)}\right] \\ \quad \text{end} \\ \text{end} \end{cases} \tag{40}$$

where N_t is the number of time steps and N_d is the number of subdomains.

4. NUMERICAL RESULTS AND DISCUSSIONS

4.1. Eigenvalue Analysis and Single Domain Result

The frequency domain discretized system is obtained from (1) and (2) assuming harmonic plane wave travels in a lossless medium

$$j\omega\mathbf{M}_{ee}\mathbf{e} - \mathbf{K}_{eb}\mathbf{b} = 0 \qquad j\omega\mathbf{M}_{bb}\mathbf{b} - \mathbf{K}_{be}\mathbf{e} = 0 \tag{41}$$

From (41), spurious eigenvalues and error convergence are analyzed. After eliminating the unknown vector $\mathbf{b}$, the eigenvalue problem of $\mathbf{e}$ can be obtained

$$\mathbf{Ye} = \omega^2\mathbf{Xe} \tag{42}$$

where

$$\mathbf{Y} = \mathbf{K}_{eb}(\mathbf{M}_{bb})^{-1}\mathbf{K}_{be} \qquad \mathbf{X} = \mathbf{M}_{ee} \tag{43}$$

The solution $\mathbf{e}$ is the eigenvector while ω^2 is the eigenvalue. A 2D PEC cavity model of TMz mode with triangle mesh shows the effectiveness of the **EB** scheme based FETD. The basis functions for **E** degenerate to nodal basis functions and volume integrations degenerate to surface integration. The cavity size is $\sqrt{3}\,\mathrm{m} \times \sqrt{2}\,\mathrm{m}$, the basis functions are **E**1**B**1, that is, first order nodal basis functions for **E** and constant normal linear tangential basis functions for **B** as shown in Fig. 1. The sampling density is 15 points per wavelength (PPW). Table 1 is the comparison between the numerical eigenvalues and the analytical eigenvalues, from which we can see that the **EB** scheme based FETD is valid in suppressing spurious modes even with the same order basis

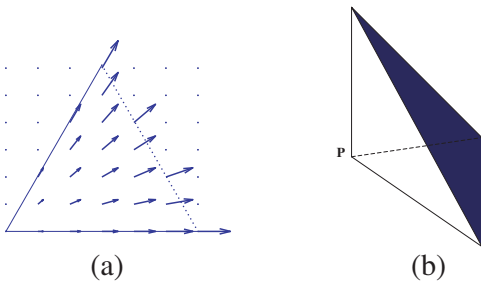

Figure 1. First order basis functions for 2D TMz case. (a) Constant normal linear tangential (CN/LT) basis function corresponding to the dot-line edge of the triangle; (b) nodal basis function (shaded part) corresponding to the vertex P of the triangle.

functions and the eigenvalue accuracy is good (first eight numerical eigenvalues are listed as examples). A pulse of Blackman-Harris window (BHW) function with characteristic frequency of 150 MHz is added as the source at the location of (0.7 m, 0.4 m), the observer is located at (0.05 m, −0.35 m) (the origin of the coordinates is at the center of the cavity). The observation time window is 50 ns. High accuracy FDTD result from commercial software Wavenology is used as the reference signal. The time domain results agree very well as shown in Fig. 2(a). The main part of the spectrum of the received signal is shown in Fig. 2(b), where the peaks agree well with the analytical resonant frequencies. Therefore, both the time domain and frequency domain results demonstrate the effectiveness of the **EB** scheme based FETD.

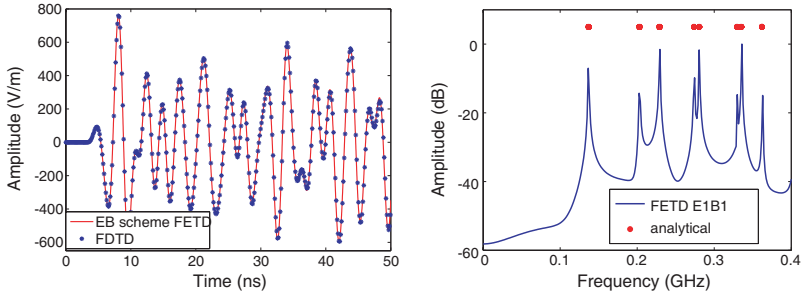

Figure 2. **EB** FETD cavity results. (a) Time domain comparison; (b) resonant frequency comparison.

Table 1. Comparison between analytical eigenvalues and **EB** scheme based FETD numerical eigenvalues.

Analytical	**EB** FETD	Error
1.36836e8	1.36880e8	3.228e-4
2.02960e8	2.03104e8	7.091e-4
2.28970e8	2.29174e8	8.900e-4
2.73672e8	2.74023e8	1.285e-3
2.80430e8	2.80809e8	1.306e-3
3.29545e8	3.30152e8	1.842e-3
3.35178e8	3.35827e8	1.938e-3
3.62034e8	3.62837e8	2.218e-3

Table 2. Comparison between **EB** scheme FETD and **EH** scheme FETD.

	E1**B**1	**E**1**H**2
Unknowns for **B**	2971	0
Unknowns for **H**	0	9838
Unknowns for **E**	926	926
Total number of unknowns	3987	10764
Time cost for 1000 leap frog steps (sec)	4.26	39.77

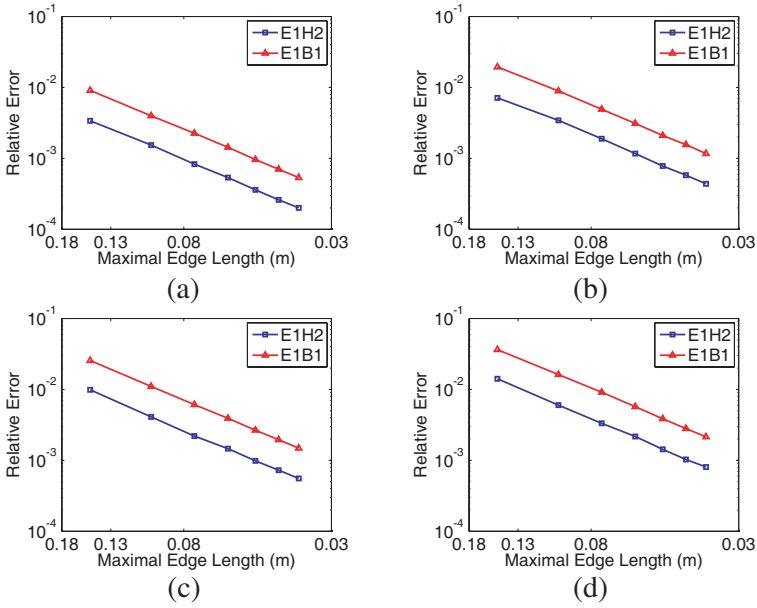

Figure 3. Relative error vs maximal edge length in log-log scale. (a) TM_{11} mode; (b) TM_{21} mode; (c) TM_{12} mode; and (d) TM_{22} mode.

Basis functions of **E**1**H**2 are needed to suppress the spurious modes if the **EH** scheme is used. With the same PEC cavity above, the relative error versus maximal edge length obtained from **E**1**H**2 and **E**1**B**1 for the first 4 modes, that is, TM_{11}, TM_{21}, TM_{12} and TM_{22}, is illustrated in Fig. 3. It is clear that both **E**1**H**2 and **E**1**B**1 have the same error convergence speed over maximal edge length of mesh, however, **E**1**B**1 is more efficient than **E**1**H**2, the comparison of the number of unknowns and time consuming with PPW = 10 is shown

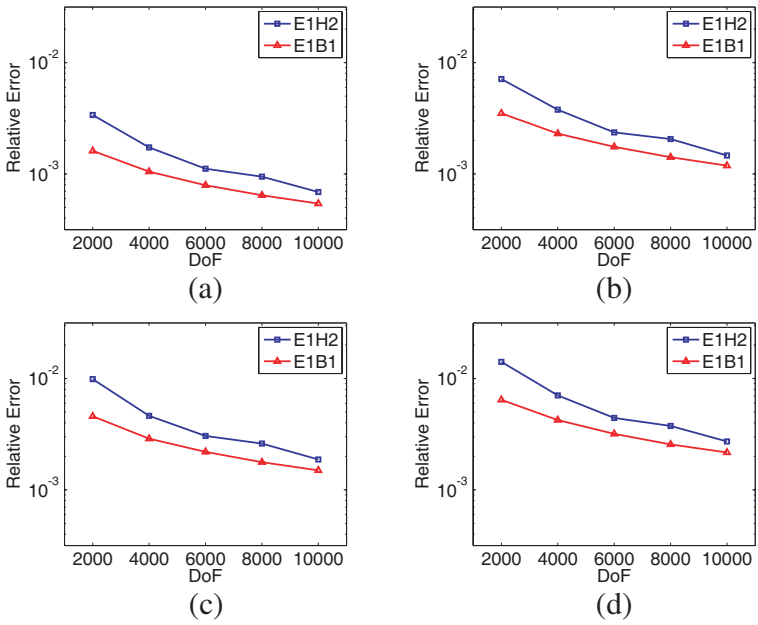

Figure 4. Relative error vs DoF. (a) TM_{11} mode; (b) TM_{21} mode; (c) TM_{12} mode; and (d) TM_{22} mode.

in Table 2. If the number of unknowns is fixed, the error in the **EB** scheme is always smaller than the **EH** scheme, as Fig. 4 shows. From Fig. 3, Fig. 4 and Table 2, we can see the advantages of **EB** scheme in computation efficiency.

4.2. A Single Domain with PML

An open region with PML is shown in Fig. 5. The square in the center is the computational region and the squares around the center one are the PML regions, which have attenuation factors

$$\omega_\eta = K_{\max}\omega\frac{|\eta-\eta_b|^p}{d^p}, \quad \eta = x, y, z \tag{44}$$

those are used in (12)–(15).

For the 2D TMz case, ω_z is zero. $\tilde{\mathbf{E}}$, $\mathbf{E}^{(1)}$, $\mathbf{E}^{(2)}$ have only $\hat{\mathbf{z}}$ component and $\tilde{\mathbf{B}}$, $\mathbf{B}^{(1)}$, $\mathbf{B}^{(2)}$ have $\hat{\mathbf{x}}$ and $\hat{\mathbf{y}}$ components. Usually $K_{\max}$ is a constant between 5 and 12, and p is the order of the attenuation factor which can be chosen from 0 to 2. d is the thickness of the PML region, η_b is the location of the interface shared by the PML region and computational region.

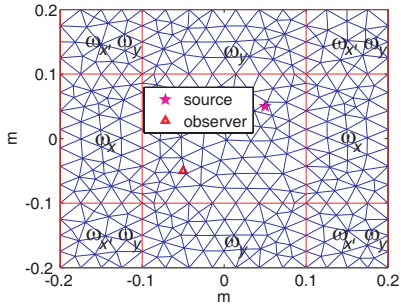

Figure 5. Mesh of an open region with PML.

The size of the computational region is $0.2\,\mathrm{m} \times 0.2\,\mathrm{m}$ with air; the source is first derivative of BHW pulse with characteristic frequency of 200 MHz located at $(0.05\,\mathrm{m}, 0.05\,\mathrm{m})$; the observer is located at $(-0.05\,\mathrm{m}, -0.05\,\mathrm{m})$. We choose $p = 1$ and $K_{\max} = 10$, and the electric field intensity at the observer is shown in Fig. 6(a). The errors of the received signals from different thickness of the PML region is shown in Fig. 6(b). It can be observed that, when $d = 0.5\,\mathrm{m}$, the error is less than 0.5%, which can be regarded as an acceptable error. As the central frequency of first derivative of BHW pulse in this case is about 300 MHz, 0.5 m is about half of the wavelength. So $\frac{\lambda}{2}$ can be an economic choice for this strongly well-posed PML thickness.

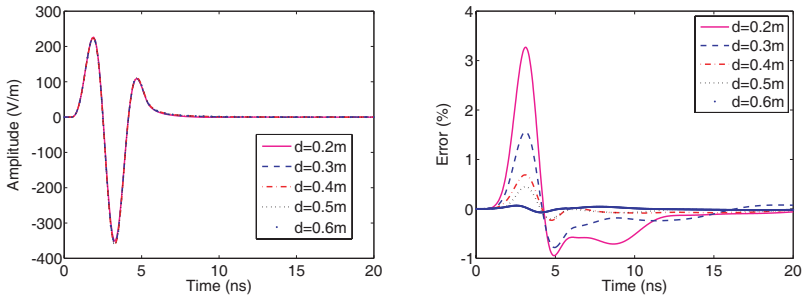

(a) (b)

Figure 6. PML performance of different thickness d. (a) Received signals; (b) relative errors (the received signal of $d = 1\,\mathrm{m}$ is chosen as the reference).

A comparison between result from FDTD (Wavenology) and result from **EB** FETD with PML thickness of $d = 0.5\,\mathrm{m}$ is shown Fig. 7. There is no reflection and the two results agree well, so the **EB** FETD with PML is effective to simulate the unbounded region.

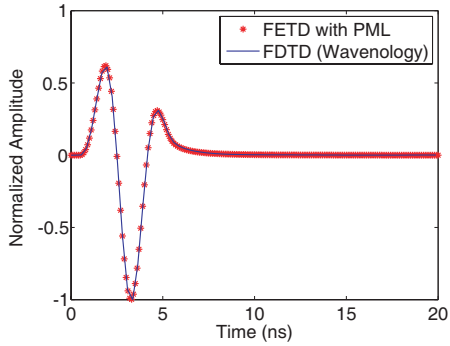

Figure 7. Comparison between **EB** scheme FETD with PML and FDTD.

4.3. DG-FETD with Multi-domains

A non-conformal TMz FETD case is investigated to verify the effectiveness and advantage of the DG-FETD method based on the **EB** scheme. The basis functions are **E**1**B**1. As shown in Fig. 8(a), the size of the PEC cavity is $1.6\,\mathrm{m} \times 1.2\,\mathrm{m}$, and it is divided into 3 subdomains. The interface locations are $x = -0.3\,\mathrm{m}$ and $x = 0.3\,\mathrm{m}$. As shown, there are two PEC objects, a rectangle and a circle. Due to the existence of these objects, a relatively fine mesh is needed. The sampling density in terms of PPW (number of points per wavelength) for the three subdomains are 8, 11 and 8, respectively. The mesh of the same case with a single domain FETD is shown in Fig. 8(b). Without domain decomposition, the whole computation region needs a fine mesh, that is, the sampling density is about 11 PPW. The source is the first derivative of BHW pulse [40] with characteristic frequency of 200 MHz located at $(-0.5\,\mathrm{m}, 0\,\mathrm{m})$, and the observer is located at $(0.5\,\mathrm{m}, 0\,\mathrm{m})$. Observation window is 50 ns. The time-domain result obtained from the proposed **EB** scheme based DG-FETD method is compared to the results from single domain FETD and FDTD methods. The computation load and accuracy comparison is in Table 3. We can see the three time domain results agree well in Fig. 9. Taking the dense meshed FDTD results as the reference solution, the L2 error of DG-FETD is less than 2 percents, that is, including the interfaces between subdomains does not obviously decrease the accuracy, compared to 1.3 percent error in that of a single domain FETD method. However, the speedup of the DG-FETD is obvious: it only takes about one fourth of the time of the single domain FETD method and about one tenth of the FDTD method. The reason lies in the following aspects: first, the

ability of meshing fine structures enables the FETD to avoid many of the wasted unknowns for the coarse part, and the time step interval can be larger than FDTD because FDTD needs small cells to catch the geometry of the fine structure; second, compared to single domain FETD, the DG-FETD can have less unknowns for the coarse mesh part via a non-conformal mesh; third, for DG-FETD, the system is divided into a few smaller ones, and the inversion of the matrices for these smaller systems is faster than the inversion of the big matrix which contains all the unknowns in the computation region. So the proposed **EB** scheme based DG-FETD method is computationally economic compared to the single domain **EB** scheme FETD and FDTD methods, and has the potential of application to large scale or/and multiscale problems with efficiency improvement over previous methods.

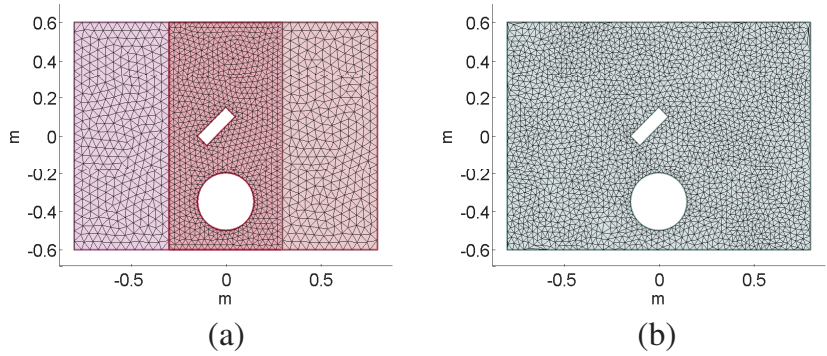

Figure 8. Mesh of the cavity. (a) DG-FETD mesh of 3 subdomains; (b) single domain FETD mesh.

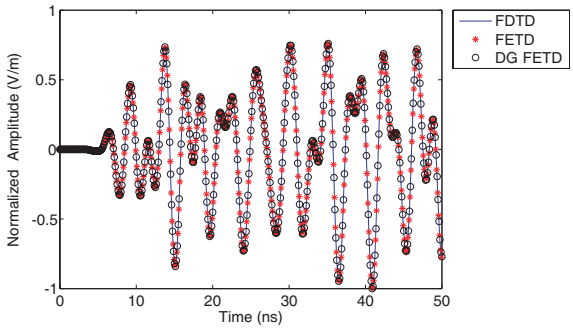

Figure 9. Time domain results comparison.

Table 3. Computational costs comparison.

	EB DG-FETD	**EB** FETD	FDTD
Maximal Δt (ps)	21.4	19.6	2.1
CPU time (sec)	4.95	22.58	51.04
DoF	5893	9392	8908
L2 error	1.892	1.371	0

5. CONCLUSION AND FUTURE WORK

In this paper, we have proposed a new FETD method for Maxwell's equations which is based on the variables **E** and **B** with Galerkin's method. Compared to the widely used **EH** scheme FETD, it can suppress the spurious modes with the same order basis functions for **E** and **B**. Therefore the total number of unknowns can be much fewer than the **EH** scheme, and the computation costs will be reduced. In addition, a strongly well-posed PML is implemented with the newly proposed **EB** scheme FETD and shown to be effective. An optimistic choice of the PML region thickness is found which can be used as an empirical reference in the future research. Then this **EB** scheme based FETD is extended to domain decomposition, where the central flux is employed to fulfill the energy communication between the adjacent subdomains. This new algorithm, **EB** scheme based DG-FETD method, is shown to be accurate and advantageous in computation loads.

The effectiveness of the algorithms developed here are demonstrated with 2D TMz numerical results, but it is straightforward to apply this to the DH based FETD and DG-FETD methods in 2D. In the following research, the new **EB** scheme based FETD can be extended to 3D cases to test the effectiveness. The advantage is expected to become even more obvious for 3D problems. As the leap frog scheme is chosen to be the time stepping scheme, the hybrid methods, such as combining FDTD with **EB** scheme based FETD, can be introduced for further enhancing computation efficiency.

REFERENCES

1. Jin, J., *The Finite Element Method in Electromagnetics*, Wiley, New York, 2007.

2. Monk, P., *Finite Element Method for Maxwells Equations*, Oxford, 2003.
3. Silvester, P. and R. Ferrari, *Finite Elements for Electrical Engineers*, Cambridge University Press, 1996.
4. Andersen, L. and J. Volakis, "Development and application of a novel class of hierarchical tangential vector finite elements for electromagnetics," *IEEE. Trans. Antennas Propagat.*, Vol. 47, No. 1, 112–120, 1999.
5. Volakis, J., T. Ozdemir, and J. Gong, "Hybrid finite-element methodologies for antennas and scattering," *IEEE. Trans. Antennas Propagat.*, Vol. 45, No. 3, 493–507, 1997.
6. Tonti, E., "Finite formulation of the electromagnetic field," *Progress In Electromagnetics Research*, Vol. 32, 1–44, 2001.
7. Polycarpou, A., P. Tirkas, and C. Balanis, "The finite-element method for modeling circuits and interconnects for electronic packaging," *IEEE Trans. Microw. Theory Techn.*, Vol. 45, No. 10, 1868–1874, 1997.
8. Lee, J., R. Lee, and A. Cangellaris, "Time-domain finite-element methods," *IEEE. Trans. Antennas Propagat.*, Vol. 45, No. 3, 430–442, 1997.
9. Jiao, D. and J. Jin, "A general approach for the stability analysis of the time-domain finite-element method for electromagnetic simulations," *IEEE. Trans. Antennas Propagat.*, Vol. 50, No. 11, 1624–1632, 2002.
10. Petersson, L. and J. Jin, "A three-dimensional time-domain finite-element formulation for periodic structures," *IEEE. Trans. Antennas Propagat.*, Vol. 54, No. 1, 12–19, 2006.
11. Vaseghi, B., N. Takorabet, and F. Meibody-Tabar, "Transient finite element analysis of induction machines with stator winding turn fault," *Progress In Electromagnetics Research*, Vol. 95, 1–18, 2009.
12. Faghihi, F. and H. Heydari, "A combination of time domain finite element-boundary integral and with time domain physical optics for calculation of electromagnetic scattering of 3-D structures," *Progress In Electromagnetics Research*, Vol. 79, 463–474, 2008.
13. Mur, G., "The finite-element modeling of three-dimensional time-domain electromagnetic fields in strongly inhomogeneous media," *IEEE Trans. Magn.*, Vol. 28, No. 2, 1130–1133, 1992.
14. Gedney, S. and U. Navsariwala, "An unconditionally stable finite element time-domain solution of the vector wave equation," *IEEE Microw. Guided Wave Lett.*, Vol. 5, No. 10, 332–334, 1995.

15. Tsai, H., Y. Wang, and T. Itoh, "An unconditionally stable extended (USE) finite-element time-domain solution of active nonlinear microwave circuits using perfectly matched layers," *IEEE Trans. Microw. Theory Techn.*, Vol. 50, No. 10, 2226–2232, 2002.
16. Jiao, D., J. Jin, E. Michielssen, and D. Riley, "Time-domain finiteelement simulation of three-dimensional scattering and radiation problems using perfectly matched layers," *IEEE. Trans. Antennas Propagat.*, Vol. 51, No. 2, 296–305, 2003.
17. Cangellaris, A., C. Lin, and K. Mei, "Point-matched time domain finite element methods for electromagnetic radiation and scattering," *IEEE. Trans. Antennas Propagat.*, Vol. 35, No. 10, 1160–1173, 1987.
18. Wong, M., O. Picon, and V. Fouad Hanna, "A finite element method based on whitney forms to solve Maxwell equations in the time domain," *IEEE Trans. Magn.*, Vol. 31, No. 3, 1618–1621, 1995.
19. Feliziani, M. and F. Maradei, "An explicit-implicit solution scheme to analyze fast transients by finite elements," *IEEE Trans. Magn.*, Vol. 33, No. 2, 1452–1455, 1997.
20. Donderici, B. and F. Teixeira, "Mixed finite-element time-domain method for transient Maxwell equations in doubly dispersive media," *IEEE Trans. Microw. Theory Techn.*, Vol. 56, No. 1, 113–120, 2008.
21. Donderici, B. and F. Teixeira, "Conformal perfectly matched layer for the mixed finite element time-domain method," *IEEE. Trans. Antennas Propagat.*, Vol. 56, No. 4, 1017–1026, 2008.
22. Yioultsis, T., N. Kantartzis, C. Antonopoulos, and T. Tsiboukis, "A fully explicit whitney element-time domain scheme with higher order vector finite elements for three-dimensional high frequency problems," *IEEE Trans. Magn.*, Vol. 34, No. 5, 3288–3291, 1998.
23. Guillouard, K., M. Wong, V. Fouad Hanna, and J. Citerne, "A new global time-domain electromagnetic simulator of microwave circuits including lumped elements based on finite-element method," *IEEE Trans. Microw. Theory Techn.*, Vol. 47, No. 10, 2045–2049, 1999.
24. Sekine, T. and H. Asai, "Mixed finite element time domain method based on iterative leapfrog scheme for fast simulations of electromagnetic problems," *IEEE International Symposium on Electromagnetic Compatibility (EMC), 2011*, 596–601, IEEE, 2011.

25. Cohen, G. and M. Durufle, "Non spurious spectral-like element methods for Maxwell's equations," *J. Comput. Math.*, Vol. 25, 282–300, 2007.
26. Winkler, J. R. and J. B. Davies, "Elimination of spurious modes in finite element analysis," *J. Computat. Phys.*, Vol. 56, 1–14, 1984.
27. Tobón, L., J. Chen, and Q. H. Liu, "Spurious solutions in mixed finite element method for Maxwell's equations: Dispersion analysis and new basis functions," *J. Computat. Phys.*, Vol. 230, No. 19, 7300–7310, 2011.
28. Chen, J., L. Tobon, M. Chai, J. Mix, and Q. H. Liu, "Efficient implicit-explicit time stepping scheme with domain decomposition for multiscale modeling of layered structures," *IEEE Trans. Compon. Packag. Manuf. Technol.*, Vol. 1, No. 9, 1438–1446, 2011.
29. Chen, J. and Q. H. Liu, "A non-spurious vector spectral element method for Maxwell's equations," *Progress In Electromagnetics Research*, Vol. 96, 205–215, 2009.
30. Cangellaris, A. and H. Wu, "Domain decomposition and multi-scale finite elements for electromagnetic analysis of integrated electronic systems," *IEEE International Symposium on Electromagnetic Compatibility (EMC), 2005*, Vol. 3, 817–822, IEEE, 2005.
31. Gedney, S., T. Kramer, C. Luo, J. Roden, R. Crawford, B. Guernsey, J. Beggs, and J. Miller, "The discontinuous Galerkin finite element time domain method (DGFETD)," *IEEE International Symposium on Electromagnetic Compatibility (EMC), 2008*, 1–4, IEEE, 2008.
32. Lu, T., W. Cai, and P. Zhang, "Discontinuous Galerkin time domain method for gpr simulation in dispersive media," *IEEE Trans. Seosci. Remote Sens.*, Vol. 43, No. 1, 72–80, 2005.
33. Gan, H. and D. Jiao, "A time-domain layered finite element reduction recovery (LAFE-RR) method for high-frequency VLSI design," *IEEE. Trans. Antennas Propagat.*, Vol. 55, No. 12, 3620–3629, 2007.
34. Canouet, N., L. Fezoui, and S. Piperno, "Discontinuous Galerkin time-domain solution of Maxwell's equations on locally-refined nonconforming cartesian grids," *COMPEL: Int. J. for Computation and Maths. in Electrical and Electronic Eng.*, Vol. 24, No. 4, 1381–1401, 2005.
35. Shi, Y. and C.-H. Liang, "Simulations of the left-handed medium using discontinuous Galerkin method based on the hybrid domains," *Progress In Electromagnetics Research*, Vol. 63, 171–191, 2006.

36. Nédélec, J., "A new family of mixed finite elements in R3," *Numerische Mathematik,* Vol. 50, No. 1, 57–81, 1986.
37. Nédélec, J., "Mixed finite elements in R3," *Numerische Mathematik*, Vol. 35, No. 3, 315–341, 1980.
38. Peterson, A., S. Ray, and R. Mittra, *Computational Methods for Electromagnetics*, Vol. 24. IEEE Press, New York, 1998.
39. Fan, G.-X. and Q. H. Liu, "A strongly well-posed PML in lossy media," *IEEE Antennas Wireless Propagat. Lett.*, Vol. 2, No. 7, 97–100, 2003.
40. Liu, Q. H., "The PSTD algorithm: A time-domain method requiring only two cells per wavelength," *Microwave and Optical Technology Letters*, Vol. 15, 158–165, 1997.